Failure mechanisms in a unidirectional fibre-reinforced thermoplastic composite under uniaxial, in-plane biaxial and hydrostatically confined compression

H. COUQUE, C. ALBERTINI*, J. LANKFORD
Southwest Research Institute, San Antonio, TX 78228, USA
**Commission of the European Communities Joint Research Centre, Ispra, Italy*

Certain practical situations require that fibre-reinforced polymeric-matrix composites be able to withstand compressive loadings parallel to the fibre direction. Recent investigations have been conducted to establish the onset of initial instability in polymeric-matrix composites subject to simple uniaxial loading [1–3]. The transferability of these results to more-complex mixed-mode compressive loading situations remains to be demonstrated. The objective of this letter is to report on the characterization of strength and damage mechanisms for a unidirectional carbon fibre-reinforced composite subject to compressive loading under hydrostatically confined uniaxial loading versus in-plane biaxial loading at nominally equivalent off-axis maximum stress levels.

The material selected for study was a poly(ether ether ketone) (PEEK) matrix and polyacrylonitrile (PAN)-derived carbon fibre-reinforced composite. The matrix was a semicrystalline thermoplastic of molecular weight approximately 23 000, the properties and microstructure of which are extremely sensitive to its thermal history. In producing the present composite the matrix was melt-impregnated at 380 °C for 30 min; subsequent heat treatment resulted in a spherulitic microstructure revealed by argon-ion etching to be of the order of 8 μm in size.

Carbon fibres (type AS4) approximately 7 μm in diameter were laid up unidirectionally, with a nominal 60% fibre density. There was a significant waviness to the fibres, i.e. uniaxial alignment was by no means perfect, and although the void density was $< 1\%$, the voids that were present tended to cluster. Both of these defects are typical of carbon fibre/PEEK composites.

Compression testing was conducted under uniaxial and biaxial loading conditions at a strain rate of about $10^{-4}\,s^{-1}$. The specimen arrangement, shown in Fig. 1a and b, minimized gripping and end-effects and favoured failure within the gauge section [1]. The material was shaped into a cylinder, 6.3 mm in diameter × 12.6 mm in length, with a reduced gauge section 5.6 mm in diameter. For conventional uniaxial compression testing, the specimen (Fig. 1a) was reinforced with internally chamfered rings, made of high-strength steel, around the bases, honed to a snug fit. A similar configuration was used for uniaxial testing under confined pressure, with the difference that the chamfered rings were a part of

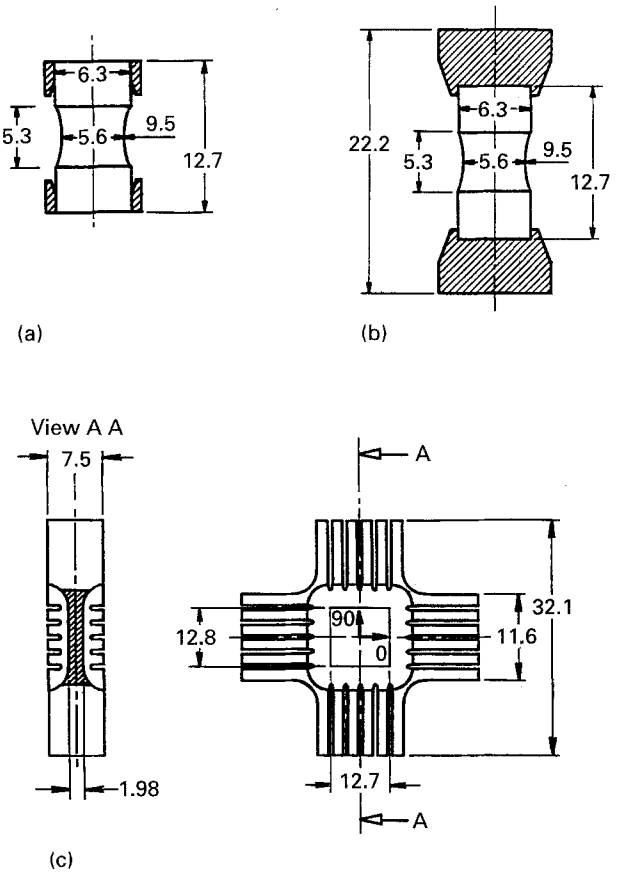

Figure 1 Compression specimen configurations: (a) uniaxial, (b) confined pressure and (c) biaxial (all units in mm).

the loading platens (Fig. 1b). This configuration permitted the application of a uniform confining pressure to the gauge section. All specimens, as well as the matching hardened steel load platens, were carefully machined so that the mating surfaces were parallel within 4 μm over the entire load surface. These uniaxial tests were performed under crosshead control in a servocontrolled hydraulic machine.

Uniaxial tests under confined pressure were conducted using a pressure vessel filled with di-2-ethyl hexyl sebacate pressure transmitting fluid at a pressure varying from 50 to 250 MPa [4]. The hydraulic ram applied axial loading through sliding O-ring seals and a bridge of four electrical resistance strain gauges inside the pressure vessel measured the axial load. Hydrostatic pressure produced a zero shift in the output of this load cell, the magnitude of which was measured and subtracted from the load

0261-8028

measurements. Hydrostatic pressure was measured by a diaphragm-type electrical pressure transducer located at the fluid inlet orifice of the pressure vessel.

Biaxial testing was conducted using a unique electromechanical biaxial testing device (Ispra, Italy) [5] employing a biaxial cruciform specimen (Fig. 1c). The specimen has a uniform gauge section 12 mm × 12 mm in area and 1.9 mm thick. Loading was accomplished in the fibre direction (0°) and normal to it (90°) with a set of bars 17.5 mm in diameter made of high-strength steel. The load was monitored using strain gauges located on the bars, and strain in the gauge section was measured by means of a 45° rosette strain gauge.

In order to establish the microstructural damage basis for the compressive behaviour of the specimens, they were sectioned, polished and examined by optical microscopy. Before sectioning, samples were mounted in epoxy to preserve the damage features during preparation.

Strength and failure strain characteristics of the composite in the 0° direction are shown in Fig. 2a and Table I. Under uniaxial loading conditions, at confining pressures ranging from ambient to 150 MPa, the composite exhibited comparable failure properties. Increasing the hydrostatic pressure to 250 MPa, a stiffer response along with a slight increase in ultimate strength was observed. A quite different response was found with the biaxial specimen, the early response of which followed a path similar to that of the uniaxial specimen tested at a confining pressure of 250 MPa. At a small strain, of the order of only 0.0015, the capacity to carry load decreased, resulting in premature (versus the uniaxial case) failure. In particular, the failure strain was lower by more than 75%, when compared with uniaxial failure strains. This was reflected in a dramatic, six-fold decrease in the axial failure stress.

The deformation response of the biaxial specimen within the two loading directions, 0° and 90°, is shown in Fig. 3. Large strains were reached in the direction perpendicular to the fibres. In this orientation the failure strain is about twice that reached in the 0° direction for the pure uniaxial case (Table I and Fig. 3).

Fig. 4a shows a macroscopic section of a uniaxial specimen tested under the highest confining pressure (250 MPa) and a shear band oriented at about 75° from the load axis is observed. A higher-magnification view of the shear band revealed it to be composed of multiple kink bands (Fig. 4b). At ambient pressure similar features were observed, as shown in Fig. 5, but in addition interlamellar fractures were present. This indicates that shear banding deformation under reduced lateral constraint favours tensile interlamellar fracture. However, it has been shown elsewhere [6] that this damage mode is an incidental effect of the shear displacement associated with breakdown of the shear kink band. Axial splitting is not the basis for the ambient versus 250 MPa pressure strength differential, which instead is a reflection of the pressure-sensitivity of the thermoplastic matrix. It is the latter which stabilizes the 0° fibres against the nucleation of an initial microkink at the site of

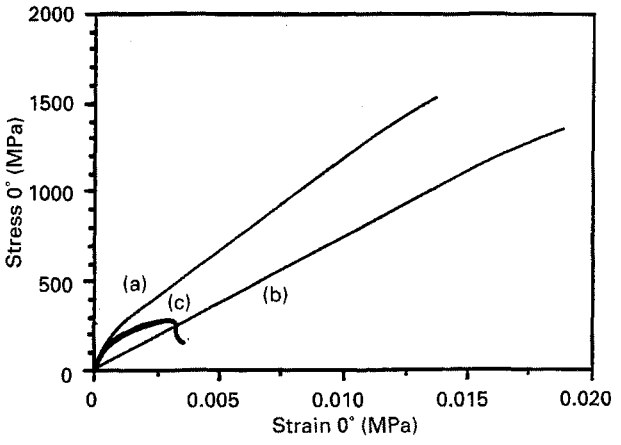

Figure 2 Engineering stress–strain response in the fibre direction for uniaxial and biaxial experiments: (a) 250 MPa (b) uniaxial (P = 0 MPa) and (c) biaxial.

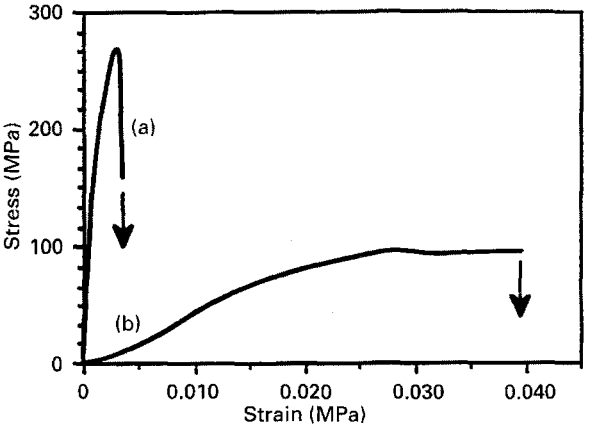

Figure 3 Engineering stress–strain response in the two loading directions for the biaxial experiment: (a) 0° and (b) 90°.

TABLE I Results of the compression tests

In-plane loading direction(s)	Hydrostatic pressure (MPa)	Compression properties		
		Direction	Compressive strength (MPa)	Failure strain
0°	0	0°	1390	0.019
0°	150	0°	1370	0.018
0°	250	0°	1540	0.014
0° and 90°	0	0°	267	0.003
0° and 90°	0	90°	97.0	0.031

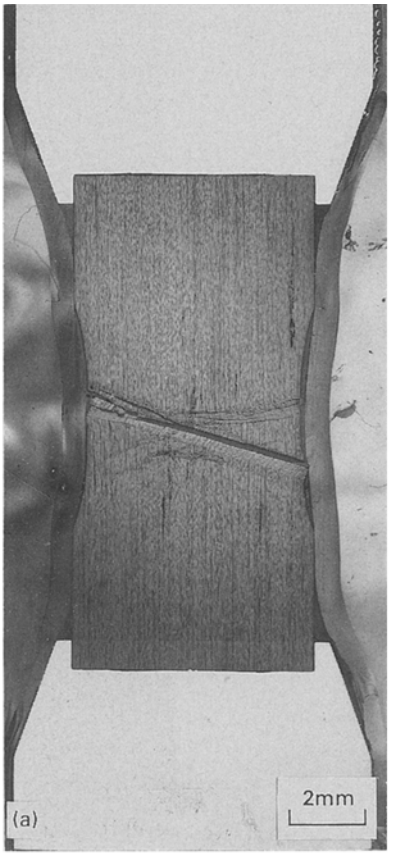

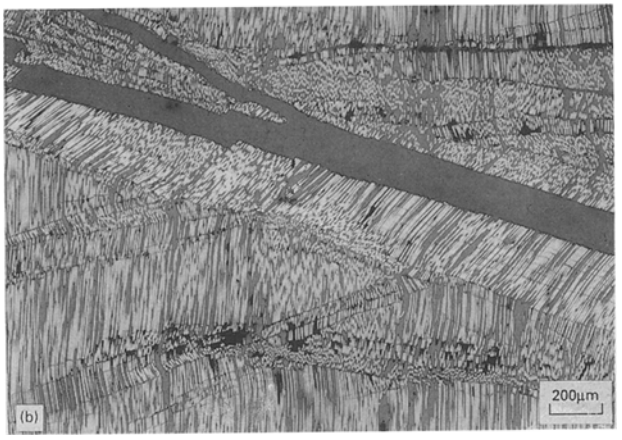

Figure 4 Section of uniaxial specimen tested at a confining pressure of 250 MPa: (a) full section and (b) detail of the shear band fracture.

highest (local) fibre misorientation. The surrounding, more axially oriented fibres tolerate high stress levels until the small volume containing the misoriented fibre(s) is activated.

In the case of the biaxial failure, on the other hand, the situation is somewhat different. As shown in Fig. 6a, the failure process of this specimen involves localized bands (arrows) parallel to the 90° loading direction. A section of one of these (section AA) is shown in Fig. 6b. This section shows that failure involved macroscale buckling within the gauge section, buckling which was approximately symmetrical about the midplane. At higher magnification (Fig. 6c) it could be seen that near the outer fibre of the sample, fibre flexure in the unfailed lower right-hand sector was intense but continuous.

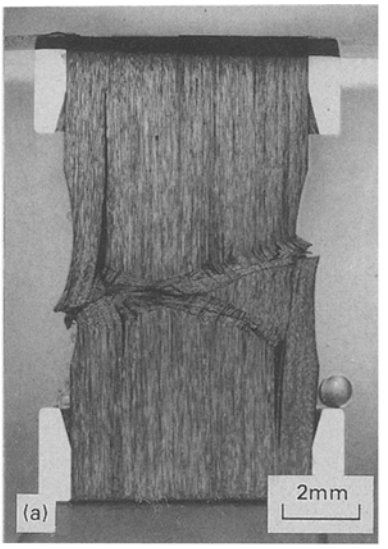

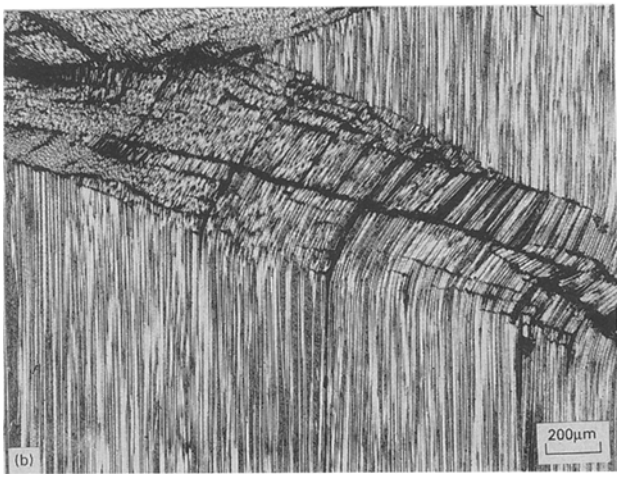

Figure 5 Section of uniaxial specimen tested under ambient pressure: (a) full section and (b) detail of the shear band fracture.

However, near the interior, fibre fracture had already occurred, nucleating several kink bands (arrows) which were in the process of moving from the interior to the surface. The latter stages of this process can be seen in the lower left-hand kink array, where the kink segments are misoriented by more than 90° in the interior (arrow A), but much less so near the surface (arrow B). Again, an interior kink nucleation event seems to have occurred.

Clearly the shear splitting took place as an aftermath of the mature kink band development, and probably constituted the failure event that terminated the region of stable load drop. The axial splitting was even less consequential, deriving simply from the wedging action of the blunt "knife" created by the catastrophic shear band fractures, which probably were also responsible for the post-failure nucleation of exterior kink bands such as those indicated by arrow C.

The most reasonable basis for low stress buckling failure during biaxial compression lies in two synergistic factors: out-of-plane compliance and the natural waviness of the fibrous lay-up. Here this does not mean highly local misalignment, such as that alluded to above as responsible for high-strength kinking, but instead the general, volumetric

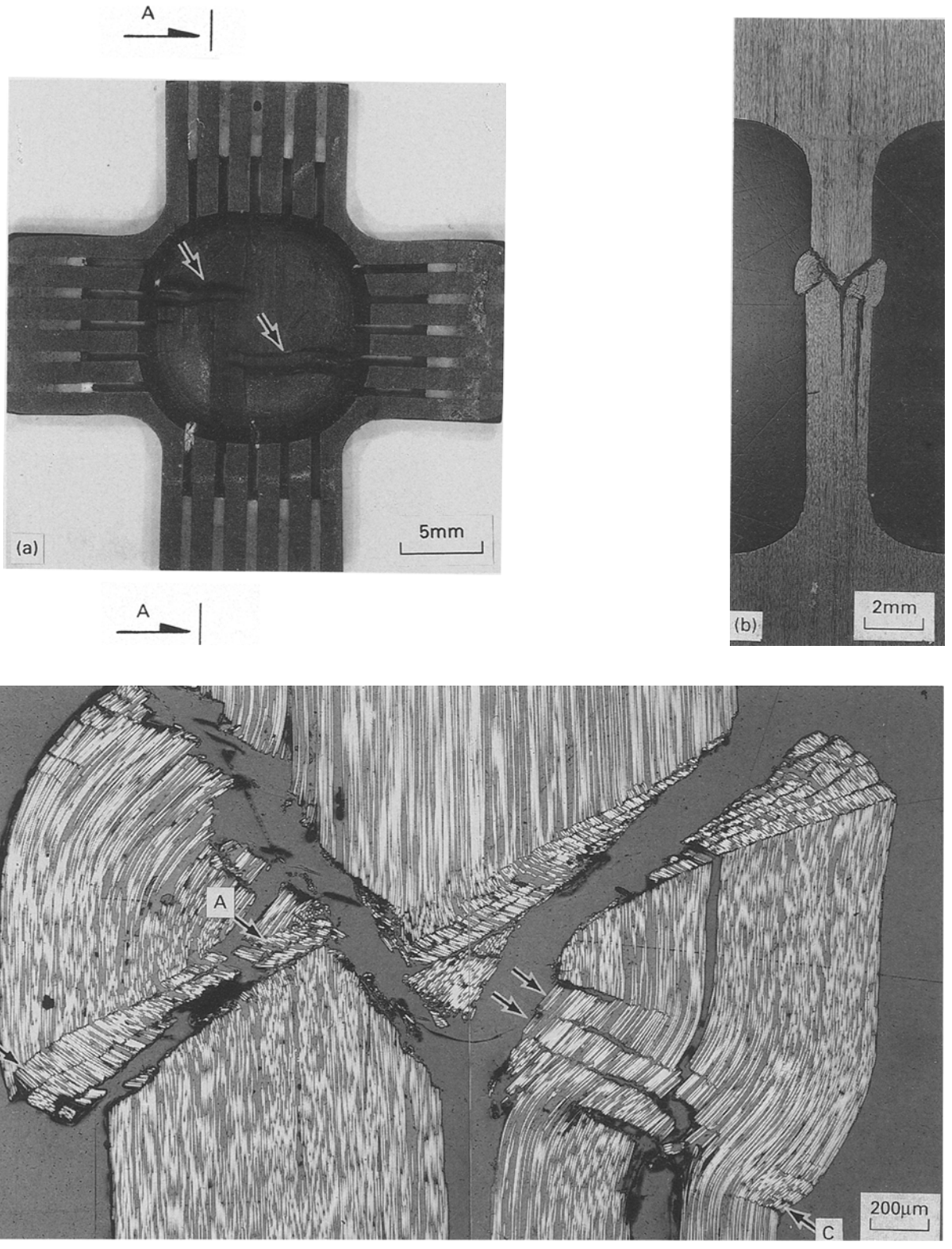

Figure 6 Biaxial damage development: (a) out-of-plane view of biaxial specimen, showing two deformation bands of 1 mm width normal to the fibre direction; (b) micrograph of the sectioned specimen (section AA); and (c) details of kink–fracture zone in (b).

waviness of a group of long fibres. In particular, there is a certain probability that somewhere in the gauge section a number of fibres will share the same wave pattern, i.e. they will be predisposed to buckle out-of-plane (the so-called shear mode), and to do so at much lower an overall stress level than that required to nucleate an axial kink. Once such an event begins to occur with rising load, the stress in the opposite side of the gauge section will rise, and produce an unrestrained gauge tendency towards buckling (outwards bulging) on that side. A structural instability has now been set up, progressing as shown in Fig. 7a, versus the more localized series of events attending a high-stress kink (Fig. 7b). It will be noted that based on bend radii, it would be anticipated that final failure will occur by the initiation of sets of internal kink bands, as observed in Fig. 6.

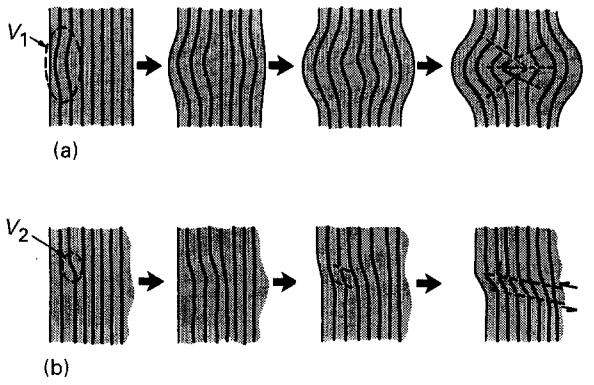

Figure 7 Schematic of compressive sequence: (a) biaxial sequence, V_1 is the volume associated with near-surface fibres preferentially aligned for shear mode of microbuckling; and (b) hydrostatic sequence, V_2 is the volume associated with misaligned fibre segment $V_1 \gg V_2$.

The situation outlined above for the biaxial case is a derivative of its essential stress asymmetry. For the cylindrical gauge section, whether confined or unrestrained, the matrix is constantly expanding radially, so regions adjacent to potential buckle sites basically move away from them, dampening their effect by denying the volumetric inflow of material required to "feed" the instability. Access to this mechanism through off-axis stress anisotropy is an effective deterrent to the attainment of the intrinsically greater ultimate strength represented by the kinking of individually misaligned fibres.

References

1. J. LANKFORD, in "Advanced composite materials", edited by M. D. Sacks (American Ceramic Society, Westerville, Ohio, 1991) p. 553.
2. A. G. EVANS and W. F. EVANS, *Acta Metall.* **26** (1978) 725.
3. M. G. DOBBS, D. G. JOHNSON and C. R. PARK, *J. Mater. Sci.* **26** (1990) 829.
4. R. ARROWOOD and J. LANKFORD, *ibid.* **22** (1987) 3737.
5. C. ALBERTINI, E. BLERY BLIONAS, M. MICUNOVIC, M. MONTAGNANI and E. V. PIZZINATO, *Inst. Phys. Conf. Ser. No. 102* (1989) 173.
6. J. LANKFORD, *J. Mater. Sci.* submitted.

Received 19 April
and accepted 9 June 1993